Parallel Pairwise Correlation Computation On Intel Xeon Phi Clusters

Yongchao Liu, Tony Pan, Srinivas Aluru
School of Computational Science & Engineering
Georgia Institute of Technology
Atlanta, GA, USA
Email: {yliu, aluru}@cc.gatech.edu; tpan7@gatech.edu

arXiv:1605.01584v1 [cs.DC] 5 May 2016

***Abstract*—Co-expression network is a critical technique for the identification of inter-gene interactions, which usually relies on all-pairs correlation (or similar measure) computation between gene expression profiles across multiple samples. Pearson's correlation coefficient (PCC) is one widely used technique for gene co-expression network construction. However, all-pairs PCC computation is computationally demanding for large numbers of gene expression profiles, thus motivating our acceleration of its execution using high-performance computing. In this paper, we present LightPCC, the first parallel and distributed all-pairs PCC computation on Intel Xeon Phi clusters. It achieves high speed by exploring the SIMD-instruction-level and thread-level parallelism within Xeon Phis as well as accelerator-level parallelism among multiple Xeon Phis. To facilitate balanced workload distribution, we have proposed a general framework for symmetric all-pairs computation by building bijective functions between job identifier and coordinate space for the first time. We have evaluated LightPCC and compared it to the sequential C++ implementation in ALGLIB (both use double-precision floating point) using a set of gene expression datasets. Performance evaluation revealed that LightPCC runs up to 20.6 and 218.2 faster than ALGLIB by using one and 16 Xeon Phi 5110P coprocesssors, respectively. In addition, LightPCC demonstrated good parallel scalability in terms of number of Xeon Phis. LightPCC is publicly available at http://lightpcc.sourceforge.net.**

***Keywords*-all-pairs computation; co-expression network; Pearson's correlation coefficient; Xeon Phi;**

I. Introduction

Co-express networks have been frequently used to reverse engineer the whole-genome interactions between complex multicellular organisms by ascertaining common regulation and thus common functions. A gene co-expression network is represented as an undirected graph with nodes being genes and edges representing significant inter-gene interactions. Such a network can be constructed by computing linear [1] or non-linear [2] co-expression measures between paired gene expression profiles across multiple samples. As the first formal and wide-spread correlation measure [3] [4] [5] [6] [7] [8] [9] [10], Pearson's correlation coefficient (PCC), or alias Pearson's r, is one frequently used technique in co-expression network construction. However, all-pairs PCC computation of gene expression profiles is not computationally trivial, especially for genome-wide association study with large number of gene expression profiles across a large population of samples. The importance of all-pairs PCC computation and its considerable computing demand motivated us to investigate its acceleration on parallel/high-performance computing architectures.

PCC statistically measures the strength of linear association between pairs of continuous random variables, but does not apply to non-linear relationship. Thus, we must ensure the linearity between paired data prior to the application of PCC. Given two random variables u and v of l dimensions each, the PCC between them is defined as

$$r(u,v) = \frac{\sum_{k=0}^{l-1}(u[k]-\bar{u})(v[k]-\bar{v})}{\sqrt{\sum_{k=0}^{l-1}(u[k]-\bar{u})^2 \sum_{k=0}^{l-1}(v[k]-\bar{v})^2}} \quad (1)$$

In Equation (1), $u[k]$ is the k-th element of u, while $\bar{u}$ is the mean of u and equal to $\frac{1}{n}\sum_{k=0}^{l-1} u[k]$. Notations are likewise defined for v. Given a variable pair, the sequential implementation of Equation (1) has a linear time complexity proportional to l. Moreover, it is known that the absolute value of the nominator is always less than or equal to the denominator [3]. Thus, $r(u,v)$ always varies in $[-1,+1]$. Concretely, $r(u,v)=0$ indicates no linear relationship, >0 positive association and <0 negative association.

Although PCC is widely used in science and engineering, the acceleration of its computation using parallel/high-performance computing architectures has not yet been extensively investigated in the literature. Chang *et al.* [11] used the CUDA-enabled GPU to accelerate all-pairs computation of PCC and computed pairwise PCC using the following standard reformulation:

$$r(u,v) = \frac{\sum_{k=0}^{l-1} u[k]\cdot v[k] - l\cdot\bar{u}\cdot\bar{v}}{\sqrt{(\sum_{k=0}^{l-1} u[k]^2 - l\cdot\bar{u}^2)(\sum_{k=0}^{l-1} v[k]^2 - l\cdot\bar{v}^2)}} \quad (2)$$

This work was extended by [12] to support GPU clusters, which adopted a master-slave model to manage workload distribution over multiple GPUs. Wang *et al.* [8] adopted a hybrid CPU-GPU coprocessing model and reformulated each variable u to a new representation w, which is defined as

$$w[k] = \frac{u[k]-\bar{u}}{|u[k]-\bar{u}|} \quad (3)$$

for each k ($0 \le k < l$) in order to benefit from general matrix-matrix multiplication (GEMM) parallelization.

In this paper, we present LightPCC, the first parallel and distributed algorithm to harness Xeon Phi clusters to accelerate all-pairs PCC computation. To achieve high speed, our algorithm explores instruction-level parallelism within SIMD vector processing units per Xeon Phi, thread-level parallelism over many cores per Xeon Phi, and accelerator-level parallelism across a cluster of Xeon Phis. Moreover, we have investigated a general framework for symmetric all-pairs computation to facilitate balanced workload distribution within and between processing elements (PEs), by building a reversible and bijective relationship between job identifier and coordinate space in a job matrix. Performance evaluation revealed that compared to the sequential C++ implementation in ALGLIB (http://www.alglib.net), our algorithm can achieve a speedup of up to 20.6 on a single Xeon Phi 5110P and up to 218.2 on 16 Xeon Phis (both algorithms used double-precision floating point). In addition, our algorithm demonstrated good parallel scalability in terms of number of Xeon Phis.

II. Xeon Phi Architecture

A Xeon Phi coprocessor is a many-core shared-memory computer [13], which runs a specialized Linux operating system and provides full cache coherency over the entire chip. The Xeon Phi is comprised of a set of processor cores, and each core offers four-way simultaneous multi-threading, i.e. 4 hardware threads per core. While offering scalar processing, each core also includes a newly-designed VPU which features a 512-bit wide SIMD instruction set architecture (ISA). Each vector register can be split to either 16 32-bit-wide lanes or 8 64-bit-wide lanes. The Xeon Phi does not provide support for legacy SIMD ISAs such as the SSE series. As for caching, each core locally has separate L1 instruction and data caches of size 32 KB each, and a 512 KB L2 cache. Moreover, all L2 caches across the entire chip are interconnected, through a bidirectional ring bus, to form a unified shared L2 cache of over 30 MB. Figure 1 gives the architectural diagram of Xeon Phis. In addition, there are two usage models for invoking Xeon Phis: offload model and native model. The offload model relies on compiler pragmas/directives to offload highly-parallel parts of an application to the Xeon Phi, while the native model treats a Xeon Phi as a symmetric multi-processing computer.

III. Parallelized Implementation

A. Pearson's Correlation Coefficient Reformulation

In the case of all-pairs computation, significantly more computation can be further reduced than pure pairwise computation. For instance, given a l-dimensional variable u, the values of $\sum_{k=0}^{l-1}(u[k]-\bar{u})$ and $\sqrt{\sum_{k=0}^{l-1}(u[k]-\bar{u})^2}$ could be repeatedly calculated up to $n-1$ times in the case of literal computing using Equation (1). Since these

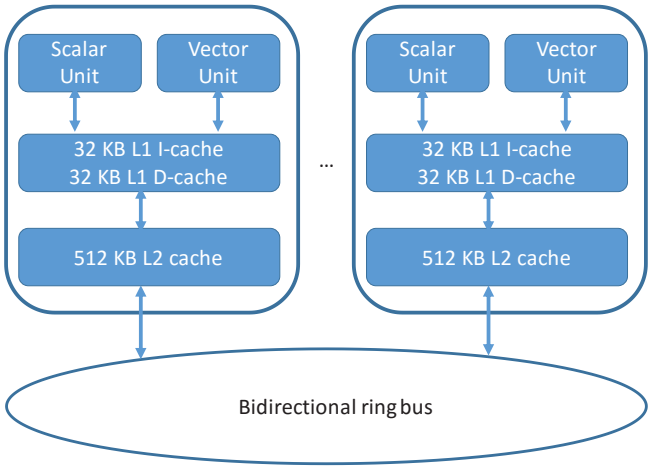


Figure 1: Architectural diagram of the Xeon Phi

two values are only dependent on u, they can be computed once beforehand. We define $X = \{X_0, X_1, \ldots, X_{n-1}\}$ to denote a set of n l-dimensional variables and compute the new representation U_i of X_i as

$$U_i[k] = \frac{X_i[k] - \bar{X}_i}{\sqrt{\sum_{k=0}^{l-1}(X_i[k] - \bar{X}_i)}} \tag{4}$$

In this way, the PCC between X_i and X_j is computed as

$$r(U_i, U_j) = \sum_{k=0}^{l-1} U_i[k] \cdot U_j[k] \tag{5}$$

From Equation (5), we can see that if organizing all members of U to form a $n \times l$ matrix A with U_i being row i of A, we can realize the all-pairs computation over U by multiplying matrix A by its transpose, i.e. $R = A \times A^T$ via a GEMM algorithm. Note that because R is symmetric, direct application of a GEMM algorithm will cause a waste of half compute power.

As mentioned above, Wang *et al.* [8] also proposed a reformulation in order to benefit from parallel GEMM algorithms (refer to Equation (3)). This reformulation computes the pairwise PCC between X_i and X_j as

$$r(U_i, U_j) = \frac{\sum_{k=0}^{l-1} U_i[k] \cdot U_j[k]}{\sqrt{\sum_{k=0}^{l-1} U_i[k]^2 \sum_{k=0}^{l-1} U_j[k]^2}} \tag{6}$$

Using this equation, though a GEMM algorithm can be used to compute the nominator, the denominator has to be additionally computed.

B. All-Pairs Computation Framework

We consider the $n \times n$ job matrix to be a 2-dimensional coordinate space on the Cartesian plane, and define the left-top corner to be the origin, the horizontal x-axis (corresponding to columns) in left-to-right direction and the vertical y-axis (corresponding to rows) in top-to-bottom direction.

1) Non-symmetric all-pairs computation: For non-symmetric all-pairs computation (non-commutative pairwise computation), the workload distribution over PEs (e.g. threads, processes, cores and etc.) would be relatively straightforward. This is because coordinates in the 2-dimensional matrix corresponds to distinct jobs. Specifically, given a coordinate (y, x) $(0 \leq x, y < n)$, we can compute its unique job identifier $J_n(y, x) \in [0, n^2)$ as

$$J_n(y, x) = yn + x \tag{7}$$

. Reversely, given a job identifier $J_n(y, x) \in [0, n^2)$, we can compute its unique coordinate as

$$\begin{array}{ll} x & = J_n(y, x)\%n \\ y & = J_n(y, x)/n \end{array} \tag{8}$$

in the job matrix.

2) Symmetric all-pairs computation: Unlike non-symmetric all-pairs computation, it suffices by only computing the upper-triangle (or lower-triangle) of the job matrix for symmetric all-pairs computation (commutative pairwise computation). In this case, balanced workload distribution could be more complex than non-symmetric all-pairs computation. For workload distribution, one approach [14] is to allocate a separate job array, totally of $n(n+1)/2$ elements if the major diagonal is counted in, with element i $(0 \leq i < n(n+1)/2)$ storing the coordinate of the i-th job and then let each PE access this array to obtain the coordinates of the jobs assigned to it. The major drawback of this approach is the extra memory consumed by the job array, since the memory overhead can be huge for large n. Another approach [8] is to use a policy designed for parallel matrix-matrix multiplication by discarding the redundant computing part, but could incur unbalanced workload distribution. In addition, some approaches (e.g. [12]) use master-slave computing model.

In this paper, we propose a general framework for workload balancing in symmetric all-pairs computation. This framework works by assigning each job a unique identifier and then building a bijective relationship between a job identifier $J_n(y, x)$ and its corresponding coordinate (y, x). This mapping is called direct bijective mapping in our context. While facilitating balanced workload distribution, this mapping merely relies on bijective functions, which is a prominent feature distinguished from existing methods. To the best of our knowledge, in the literature bijective functions have not ever been proposed for workload balancing in symmetric all-pairs computation. In [15], the authors used a very similar job numbering approach to ours in this study, but did not manage to derive a bijective function for symmetric all-pairs computation. In particular, our bijective functions are well suited to parallel algorithms on processors or accelerators with hardware schedulers (e.g. GPUs and FPGAs). Moreover, this framework can be applied to the cases with identical (e.g. our study) or varied workload per job. Without loss of generality, in the following we will interpret our framework relative to the upper triangle of the job matrix by counting in the major diagonal. Nonetheless, this framework can be easily adapted to the cases excluding the major diagonal.

3) Direct bijective mapping: Given a job (y, x) in the upper triangle, we compute its integer job identifier $J_n(y, x)$ as

$$J_n(y, x) = F_n(y) + x - y, \quad 0 \leq y \leq x < n \tag{9}$$

for n variables. In this equation, $F_n(y)$ is the total number of cells preceding row y in the upper triangle and is computed as

$$F_n(y) = \frac{y(2n - y + 1)}{2} \tag{10}$$

where y varies in $[0, n]$ and there are two boundary cases needing to be paid attention to: one is when $y = 0$ and the other is when $y = n$. When $y = 0$, $F_n(0) = 0$ because no cell in the upper triangle appears before row 0; and when $y = n$, $F_n(n) = n(n+1)/2$ because all cells in the upper triangle are included. In this way, we have defined Equation (9) based on our job numbering policy, i.e. all job identifiers vary in $[0, n(n+1)/2)$ and jobs are sequentially numbered left-to-right and top-to-bottom in the upper triangle (see Figure 2 for an example).

Reversely, given a job identifier $J = J_n(y, x)$ $(0 \leq J < n(n+1)/2)$, we need to compute the coordinate (y, x) in order to locate the corresponding variable pair. As per our definition, we have

$$\begin{cases} J \geq F_n(y) \Leftrightarrow y^2 - (2n+1)y + 2J \geq 0 \\ J \leq F_n(y+1) - 1 \Leftrightarrow y^2 - (2n-1)y + 2(J+1) - 2n \leq 0 \end{cases} \tag{11}$$

It needs to be stressed that there is surely an integer value y satisfying these two inequalities based our job numbering policy mentioned above. By solving $J \geq F_n(y)$, we get

$$y \leq n + 0.5 - \sqrt{n^2 + n + 0.25 - 2J} \tag{12}$$

This is because (i) $n^2 + n + 0.25 > 2J$ and thus $J = F_n(y)$ has two distinct y solutions theoretically, and (ii) all $0 \leq y < n$ values are to the left of the symmetric axis $y = n + 0.5$, meaning strictly monotonically decreasing as a function of y. Meanwhile, by solving $J \leq F_n(y+1) - 1$, we get

$$y \geq n - 0.5 - \sqrt{n^2 + n + 0.25 - 2(J+1)} \tag{13}$$

Similarly, this is because (i) $n^2 + n + 0.25 > 2(J+1)$ and thus $J = F_n(y+1) - 1$ has two distinct y solutions theoretically, and (ii) all $0 \leq y < n$ values are to the left of the symmetric axis $y = n - 0.5$, meaning strictly monotonically decreasing as a function of y.

In this case, by defining

$$\Delta = \sqrt{n^2 + n + 0.25 - 2(J+1)}$$

,

$$\Delta' = \sqrt{n^2 + n + 0.25 - 2J}$$

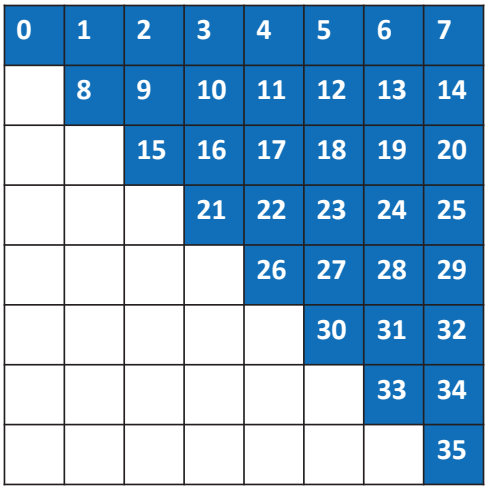


Figure 2: An example direct bijective mapping between job identifier and coordinate space

and

$$z = n - 0.5 - \sqrt{n^2 + n + 0.25 - 2(J+1)}$$

, we can reformulate Equations (12) and (13) to be

$$z \leq y \leq z + 1 + \Delta - \Delta'$$

. In this case, because $\Delta < \Delta'$, we know that $[z, z+1+\Delta-\Delta']$ is a sub-range of $[z, z+1)$ and thereby have $z \leq y < z+1$. As mentioned above, as a function of integer y, Equation (11) definitely has y solutions as per our definition, meaning that at least on integer exists in $[z, z+1+\Delta-\Delta']$, which satisfies Equation (11). Meanwhile, it is known that there always exists one and only one integer in $[z, z+1)$ (can be easily proved) and this integer equals $\lceil z \rceil$, regardless of the value of z. Since $[z, z+1+\Delta-\Delta']$ is a sub-range of $[z, z+1)$, we can conclude that Equation (11) has a unique solution y that is computed as

$$y = \lceil z \rceil = \left\lceil n - 0.5 - \sqrt{n^2 + n + 0.25 - 2(J+1)} \right\rceil \quad (14)$$

Having got y, we can compute the coordinate x as

$$x = J + y - F_n(y) \quad (15)$$

based on Equation (9).

It needs to be stressed that in addition to the aforementioned theoretical proof, we also wrote a computer program to test its correctness using a set of n values in practice. This program works as follows. For a specific n, given any coordinate (y, x) in the upper triangle, we compute a job identifier J using Equation (9). Because the job identifier corresponding to the coordinate (y, x) is known beforehand (recalling our sequential job numbering), we compare the gold-standard job identifier with the computed J. If they are unequal, the bijective mapping is wrong and otherwise, we continue to the next step. Subsequently, we reversely compute a new coordinate (y', x') from J using Equations (14) and (15). If the coordinate (y', x') is identical to its (y, x), the bijective mapping is correct and otherwise, wrong. Through our tests, the bijective functions work correctly.

C. Tiled Computation on Xeon Phi

Tiled computation is a frequently used technique in various applications accelerated by accelerators such as Cell/BEs [16], GPUs [17] and Xeon Phis [18]. This technique partitions a matrix into a non-overlapping set of equal-sized $t \times t$ tiles. In our case, we partition the job matrix and produce a tile matrix of size $m \times m$ tiles, where m equals $\lceil n/t \rceil$. In this way, all jobs in the upper triangle of the job matrix are still fully covered by the upper triangle of the tile matrix. By treating a tile as a unit, we can assign a unique identifier to each tile in the upper triangle of the tile matrix and then build bijective functions between tile identifiers and tile coordinates in the tile matrix, similarly as we do for the job matrix.

1) Computing tile coordinates: As mentioned above, we have proposed a bijective mapping between job identifier and coordinate space. Because the tile matrix has an identical structure with the original job matrix, we can directly apply our aforementioned bijective mapping to the tile matrix. In this case, given a coordinate (y_t, x_t) $(0 \leq y_t \leq x_t < m)$ in the upper triangle of the tile matrix, we can compute a unique tile identifier $J_m(y_t, x_t)$ as

$$J_m(y_t, x_t) = F_m(y_t) + x_t - y_t, \quad 0 \leq y_t \leq x_t < m \quad (16)$$

where $F_m(y_t)$ is defined similar to Equation (10) as

$$F_m(y_t) = \frac{y_t(2m - y_t + 1)}{2} \quad (17)$$

Likewise, given a tile identifier J_t $(0 \leq J_t < m(m+1)/2)$, we can reversely compute its unique vertical coordinate y_t as

$$y_t = \left\lceil m - 0.5 - \sqrt{m^2 + m + 0.25 - 2(J_t+1)} \right\rceil \quad (18)$$

and subsequently its unique horizontal coordinate x_t as

$$x_t = J_t + y_t - F_m(y_t) \quad (19)$$

2) Computing a tile: Having got the coordinate (y_t, x_t) of a tile, we can determine the coordinate range of all jobs per tile, relative to the original job matrix. More specifically, the vertical coordinate y lies in $[y_t \times t, (y_t+1) \times t)$ and the horizontal coordinate x in $[x_t \times t, (x_t+1) \times t)$. Consequently, the computation of a tile can be completed by looping over the coordinate ranges of both y and x. Note that the jobs whose coordinate $y > x$ do not need to be computed since they lie beyond the upper triangle of the job matrix. We have given the pseudocode of a sequential tiled implementation in Algorithm 1.

Algorithm 1 Pseudocode of sequential tiled computation

```
1:  procedure PEARSONR(U, R, ...)
2:      for (J_t = 0; J_t < m(m+1)/2; ++J_t) do
                                  ▷ Compute the tile coordinate (y_t, x_t)
3:          y_t = ⌈m − 0.5 − sqrt(m^2 + m + 0.25 − 2(J_t + 1))⌉
4:          x_t = J_t + y_t − y_t(2m − y_t + 1)/2
                                  ▷ Compute the tile
5:          for (y = y_t × t; y < min{n, (y_t + 1) × t}; ++y do
6:              for (x = x_t × t; x < min{n, (x_t + 1) × t}; ++x) do
7:                  if y ≤ x then
8:                      r = 0
9:                      for (k = 0; k < l; ++k) do
10:                         r += U_y[k] · U_x[k]
11:                     end for
12:                     R[y][x] = r
13:                 end if
14:             end for
15:         end for
16:     end for
17: end procedure
```

3) Multithreaded implementation: For all-pairs PCC computation, every job has the same amount of computation. In this case, the ideal load balancing policy is supposed to distributing identical number of jobs onto each PE. Herein, a thread on the Xeon Phi is referred to as a PE. From section II, we know that each core on the Xeon Phi has four hardware threads and a two-level private L1/L2 cache hierarchy with caches being connected via a bidirectional ring bus to provide coherent caching on the entire chip. This non-uniform cache access reminds us that we should keep the active hardware threads per core sharing as much data as possible with the intention to improve caching performance. In these regards, our tiled computation schedules a tile to t threads and lets these t threads to compute the tile in parallel. Note that we must guarantee that the number of threads is a multiple of t within the parallel region of our Xeon Phi kernel.

Algorithm 2 shows the pseudocode of the Xeon Phi kernel of our tiled computation. Due to the limited amount of device memory, we are not able to entirely reside the resulting $n \times n$ correlation matrix R in the Xeon Phi. To address this problem, we partition the title identifier range $[0, m(m+1)/2)$ into a set of equal-sized non-overlapping sub-ranges and adopt a multi-pass execution model by letting one pass compute one sub-range, denoted by $[J_{start}, J_{end})$ for simplicity. To match this execution model, a result buffer R' of size $(J_{end} - J_{start}) \times t^2$ elements is allocated on the Xeon Phi and used to store the results of the $J_{end} - J_{start}$ tiles. For each tile, its t^2 results are consecutively placed in R'. Once a pass finishes, we transfer R' to the host, then extract the results per tile and finally store them in the resulting matrix R allocated on the host.

To benefit from the wide 512-bit SIMD vector instructions, we have aligned each l-dimensional variable in U to 64-byte memory boundary on the Xeon Phi. In Algorithm 2, compiler directives are used to hint to the compiler to auto-vectorize the inner-most loop (lines 18 and 20 in Algorithm 2). Alternatively, we also manually vectorized the loop using SIMD instrinsic functions. The SIMD instrinsic functions used are

- _mm512_setzero_ps/pd
- _mm512_load_ps/pd
- _mm512_fmadd_ps/pd
- _mm512_mask3_fmadd_ps/pd
- _mm512_reduce_add_ps/pd

for single/double-precision float point. Interestingly, our manual-vectorization did not demonstrate obvious/significant performance advantage to auto-vectorization, through our evaluations. More specifically, our manual-vectorization does run faster than auto-vectorization, but only by a tiny margin, on a single Xeon Phi. Considering that auto-vectorization is more portable than hard-coded SIMD intrinsic functions, we have used auto-vectorization all through our implementations.

Algorithm 2 Pseudocode of the Xeon Phi kernel of our tiled computation

```
1:  procedure MTPEARSONR(U, R', J_start, J_end, ...)
2:      #pragma omp parallel
3:      {
4:      numGroups = omp_get_num_threads()/t
5:      tid = omp_get_thread_num()%t
6:      gid = omp_get_thread_num()/t
7:      for (J_t = J_start + gid; J_t < J_end; J_t += numGroups) do
                                  ▷ Compute the tile coordinate (y_t, x_t)
8:          y_t = ⌈m − 0.5 − sqrt(m^2 + m + 0.25 − 2(J_t + 1))⌉
9:          x_t = J_t + y_t − y_t(2m − y_t + 1)/2
                                  ▷ Compute offset d in R'
10:         d = (J_t − J_start) × t^2 + tid
                                  ▷ Compute its own x
11:         x = x_t × t + tid
12:         if (x < n) then
13:             for (y = y_t × t; y < min{n, (y_t + 1) × t}; ++y) do
14:                 r = 0
15:                 if (y ≤ x) then
16:                     #pragma vector aligned
17:                     #pragma simd reduction(+:r)
18:                     for (k = 0; k < l; ++k) do
19:                         r += U_x[k] · U_y]k]
20:                     end for
21:                 end if
22:                 R'[d] = r
23:                 d += t
24:             end for
25:         end if
26:     end for
27:     } //parallel region
28: end procedure
```

4) Asynchronous kernel execution: As mentioned above, we rely on multiple passes of kernel execution to complete all-pairs computation. Conventionally, having completed one pass, we transfer the newly computed results to the host, and do not initiate a new kernel execution until having completed the processing of the new results. In this way, the co-processor will be kept idle, while we transfer and process the results on the host side. A better solution would be to employ asynchronous kernel execution, which enables concurrent execution of host-side tasks and device-side kernel execution. Fortunately, the offload model provides the `signal` and `wait` clauses to support for asynchronous data transfer and kernel execution. More specifically, the `signal`

clause enables asynchronous data transfer in `#pragma offload_transfer` directives and asynchronous computation in `#pragma offload` directives. The `wait` clause blocks the current execution until an asynchronous data transfer or computation is complete. Note that the `signal` and `wait` clauses are associated with each other via a unique value. In our implementation, we have used a double-buffering approach to facilitate asynchronous computation. Algorithm 3 gives the pseudocode of our asynchronous implementation.

Algorithm 3 Pseudocode of our asynchronous execution

```
1:  procedure ASYNCKERNELEXECUTION
2:      J_stop = m(m + 1)/2
3:      J_start = 0
4:      J_end = min{J_stop, J_start + maxNumTilesPerPass}
                                  ▷ Initiate asynchronous kernel execution
5:      #pragma offload target(mic:id) signal (&signalVar) ···
6:      {mtPearsonR(U, R'_in, J_start, J_end)}
                                  ▷ Enter the core loop
7:      while (1) do
                  ▷ Wait for the kernel to complete and swap the buffers
8:          #pragma offload target(mic:id) wait (&signalVar) ···
9:          {swap(R'_in, R'_out)}
10:         swap(R'_in, R'_out)
                  ▷ Save the previous range of tile identifiers
11:         J'_start = J_start
12:         J'_end = J_end
13:         if (J_end ≥ J_stop) then
14:             break
15:         end if
                  ▷ Initiate asynchronous kernel execution
16:         J_start += maxNumTilesPerPass
17:         J_end = min{J_stop, J_start + maxNumTilesPerPass}
18:         #pragma offload target(mic:id) signal (&signalVar) ···
19:         {mtPearsonR(U, R'_in, J_start, J_end)}
                  ▷ Process the results of the completed kernel
20:         num = (J'_end − J'_start) × t^2
21:         Transfer num elements in R'_out from device to host
22:         Process the newly computed results on the host
23:     end while
                  ▷ Process the results of the completed kernel
24:     num = (J'_end − J'_start) × t^2
25:     if (num > 0) then
26:         Transfer num elements in R'_out from device to host
27:         Process the newly computed results on the host
28:     end if
29: end procedure
```

D. Distributed Computing

On Xeon Phi clusters, two distributed computing models can be used to develop parallel and distributed algorithms. One model is MPI offload model, which launches MPI processes just as an ordinary CPU cluster does. The difference is that one or more Xeon Phi coprocessors will be associated to a parental MPI process and this parental process will utilize offload pragmas/directives to interact with the affiliated Xeon Phis. In this model, communications between Xeon Phis have to be explicitly managed by their parental processes and it is not a necessity for Xeon Phis to be aware of the existence of remote communications between MPI processes. The other model is symmetric model, which treats a Xeon Phi coprocessor as a regular computer interconnected to form a compute cluster. One advantage of symmetric model to MPI offload model is that symmetric model allows for the execution of existing MPI programs designed for CPU clusters to be directly executed on Xeon Phi clusters, with no need of re-programming the code. Nonetheless, considering different architectural features between CPUs and Xeon Phis, some amount of efforts may have to be devoted to performance tuning on Xeon Phi clusters.

In our algorithm, we have used MPI offload model and also require one-to-one correspondence between MPI processes and Xeon Phis. This pairing is straightforward for the cases launching one MPI process into one node. However, it would become more complex when a nodes has multiple Xeon Phis available and multiple processes running. This is because multiple processes launched into the same node have no idea about which Xeon Phi should be associated to themselves. To address this problem, we have used the registration-based management mechanism used by [18] for paring MPI processing and Xeon Phis.

Our distributed implementation is also based on tiled computation on the Xeon Phi. Given p MPI processes, we evenly distribute tiles onto the p processes with the i-th ($0 \leq i < p$) process assigned to compute the tiles whose identifiers are in $[i \times \lceil m(m+1)/2p \rceil, (i+1) \times \lceil m(m+1)/2p \rceil)$. Within each process, we adopt the same asynchronous control workflow with the computation for single Xeon Phis (see Algorithm 3) and execute the same tiled computation kernel on the affiliated Xeon Phi in each pass (see Algorithm 2). Note that the initialization of variables J_{start} and J_{stop} (lines 2∼3 in Algorithm 3) must be changed accordingly for each process. Concretely, p_i should initialize J_{start} to be $i \times \lceil m(m+1)/2p \rceil$, and J_{stop} to be $(i+1) \times \lceil m(m+1)/2p \rceil$.

E. Variable Transformation on Xeon Phi

As mentioned above, we reformulate the computation of PCC by transforming each original variable X_i to a new representation U_i based on Equation (4). This variable transformation for input set X only needs to be done once beforehand, and is also embarrassingly parallel since the transformation per variable is mutually independent. On the other hand, each variable requires identical amount of computation since these variables have the same dimension. In these regards, we parallelize the variable transformation by evenly distributing variables onto all threads on the Xeon Phi.

Algorithm 4 gives the pseudocode of the Xeon Phi kernel of our variable transformation. In Algorithm 4, for each variable X_i the transformation consists of three steps. Step 1 (lines 7∼13) computes the mean of all elements in X_i and requires l unit arithmetic operations. Step 2 (lines 14∼20) computes the variance of all elements and takes $2l$ unit arithmetic operations if considering a square root operation as a unit. Step 3 (lines 21∼25) finishes the transformation of X_i to U_i and also needs $2l$ unit arithmetic operations. Therefore, the total computational cost of variable transformation can be estimated as $5l$ unit arithmetic operations. On

the other hand, for symmetric all-pairs computation using Equation (5), its computational cost can be estimated to be $ln(n+1)/2$ unit arithmetic operations. Consequently, the overall computational cost of our method can be estimated to be $5ln + ln(n+1)/2$ unit arithmetic operations.

Algorithm 4 Pseudocode of the Xeon Phi kernel of our variable transformation

```
1:  procedure VARIABLETRANSFORMATION((X, U))
2:      #pragma omp parallel
3:      {
4:      tid = omp_get_thread_num()
5:      chunk = ⌈ n / omp_get_num_threads() ⌉
6:      for (i = tid × chunk; i < min{n, (tid + 1) × chunk}; ++ i) do
                                                  ▷ Compute the mean
7:          mean = 0
8:          #pragma vector aligned
9:          #pragam simd reduction(+:mean)
10:         for (k = 0; k < l; ++ k) do
11:             mean+ = X_i[k]
12:         end for
13:         mean/ = l
                                                  ▷ Compute the variance
14:         variance = 0
15:         #pragma vector aligned
16:         #pragam simd reduction(+:variance)
17:         for (k = 0; k < l; ++ k) do
18:             variance+ = (X_i[k] − mean)^2
19:         end for
20:         variance = 1.0 / √variance
                                                  ▷ Compute U_i (in place)
21:         #pragma vector aligned
22:         #pragam simd
23:         for (k = 0; k < l; ++ k) do
24:             U_i[k] = (X_i[k] − mean) × variance
25:         end for
26:     end for
27:     }//parallel region
28: end procedure
```

IV. Performance Evaluation

We evaluated LightPCC from the following two perspectives: (i) performance comparison with the sequential C++ implementation in the ALGLIB library (version 3.10.0) and (ii) parallel scalability evaluation on a Xeon Phi cluster. Since the runtime of PCC computation is only subject to n and l, we have used a set of gene expression profiles with each profile containing randomly generated numbers in $[0, 1]$. We have generated three gene expression datasets with n equal to 16000 (16K), 32000 (32K) or 64000 (64K) and $l = 5000$ (5K). All tests are conducted on 8 compute nodes in CyEnce HPC Cluster (Iowa State University) with each node having two Intel E5-2650 8-core 2.0 GHz CPUs, two Xeon Phi 5110P coprocessors (60 cores and 8 GB memory) and 128 GB memory. Both LightPCC and ALGLIB are compiled by Intel C++ compiler v15.0.1 with option `-fast` enabled. Meanwhile, when two processes run in a node, we used the environment variable `I_MPI_PIN_PROCESSOR_LIST` to guide Intel MPI runtime system to pin two processes per node to distinct CPUs (recall that we have two CPUs per node).

We first evaluated the performance of LightPCC and ALGLIB (i.e. the `alglib::pearsoncorrm` subroutine) using the aforementioned three gene expression datasets. For our algorithm, we set the tile size to 4×4 (i.e. $t = 4$) and configure each core to run four hardware threads associated with the `compact` OpenMP thread affinity mode (i.e. 236 actives threads on 59 cores). This means that we schedule one tile to a core at a time, and let all four threads per core compute the same tile in parallel, with one thread processing one column. In this way, the four threads per core will access the same row variable simultaneously, thereby improving data sharing. It needs to be stressed that because ALGLIB uses double-precision floating point, LightPCC used double precision as well for fair comparison.

Table I: Runtimes and speedups over ALGLIB

Program	Time (s)			Speedup		
	16K	32K	64K	16K	32K	64K
ALGLIB	355.0	1451.1	5891.6	–	–	–
1 Phi	27.4	83.2	285.4	12.9	17.4	20.6
2 Phis	15.6	55.5	203.7	22.8	26.2	28.9
4 Phis	7.8	29.6	103.8	45.7	49.1	56.8
8 Phis	3.9	15.1	52.4	90.2	96.1	112.5
16 Phis	2.2	7.6	27.0	160.1	190.2	218.2

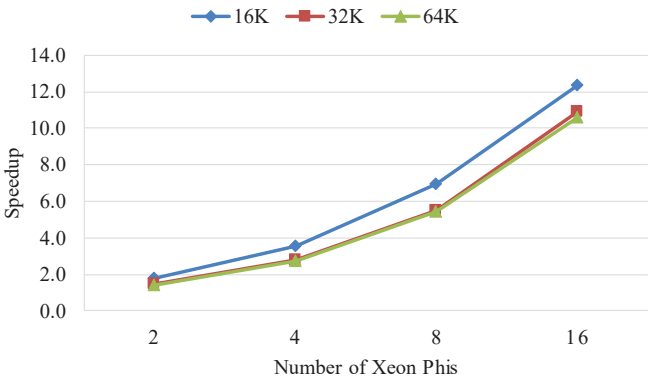


Figure 3: Parallel scalability evaluation

Table I shows the performance comparison between LightPCC and ALGLIB. In this test, each program was executed five times and the runtime is computed by averaging the five executions. From the table, it can be observed that the speedup of LightPCC over ALGLIB gradually increases as n grows larger for each case. Specifically, compared to ALGLIB, LightPCC runs $12.9\times$, $17.4\times$ and $20.6\times$ faster using one Xeon Phi and $160.1\times$, $190.2\times$, and $218.2\times$ faster using 16 Xeon Phis for n=16K, n=32K and n=64K, respectively.

Subsequently, we evaluated the parallel scalability of our algorithm with respect to varied number of Xeon Phis (see Figure 3). On average, LightPCC achieves a speedup of 1.6 using 2 Xeon Phis, 3.0 using 4 Xeon Phis, 6.0 using 8 Xeon Phis and 11.3 using 16 Xeon Phis, compared to execution using one Xeon Phi. Accordingly, the maximum speedup is 1.8, 3.5, 7.0 and 12.4 respectively.

V. Conclusion

PCC is a correlation measure that investigates the relationship between two continuous random variables and has been widely used in Bioinformatics. For instance, one popular application is to compute the correlation between gene expression profiles and then build a gene co-expression network to identify common regulation and thus common functions [19]. This network construction can be realized by means of all-pairs computation between gene expression profiles. This is computationally demanding for large co-expression network construction at a genome-wide scale.

In this paper, we have presented LightPCC, the first parallel and distributed all-pairs PCC computation algorithm on Xeon Phi clusters, which harnesses three levels of parallelism (i.e. SIMD-instruction-level parallelism, thread-level parallelism and accelerator-level parallelism) to achieve high performance. Furthermore, we have proposed a general framework for workload balancing in symmetric all-pairs computation. This framework assigns unique identifiers to jobs in the upper triangle of the job matrix and builds bijective functions between job identifier and coordinate space. We have evaluated the performance of our algorithm using a set of gene expression profiles and further compared this performance to a sequential C++ implementation in ALGLIB (both algorithms use double-precision floating point). Our experimental results showed that compared to ALGLIB, LightPCC runs up to $20.6\times$ faster on one Xeon Phi 5110P, and up to $218.2\times$ faster on 16 Xeon Phis. In addition, our algorithm yielded good parallel scalability with respect to varied number of Xeon Phis.

As part of our future work, we plan to apply this work to construct genome-wide gene expression network (e.g. from conventional microarray data [20], emerging RNA-seq data [21] [22], diverse genomic data [23] and so on) and then integrate it with statistical and graph analysis methods to identify critical pathways. Finally, our current implementation does not distribute PCC computation onto CPU cores. In this regard, we expect to further boost performance by employing a CPU-Phi coprocessing model that distributes workloads onto both CPUs and Xeon Phis based on their relative compute power.

Finally, besides co-expression network construction, PCC can be used to feature selection based on feature ranking in machine learning [24] [7]. In this context, PCC can be used to measure feature-class or feature-feature relevancy. When two features are perfectly correlated, it suffices by using only one feature to represent the data. In other words, one feature can be deemed as redundant since it does not provide any extra information than the other. By reducing irrelevant and redundant features without incurring much loss of information, we can reduce the computational cost and even improve downstream analysis performance. However, note that the computation of feature-class or feature-feature correlation is also not computationally trivial, especially for the cases with larger numbers of features and samples (e.g. text-document classification [25] [26]).

Acknowledgment

This research is supported in part by US National Science Foundation under IIS-1416259.

References

[1] A. J. Butte and I. S. Kohane, "Unsupervised knowledge discovery in medical databases using relevance networks." in *Proceedings of the AMIA Symposium*. American Medical Informatics Association, 1999, p. 711.

[2] J. Zola, M. Aluru, A. Sarje, and S. Aluru, "Parallel information-theory-based construction of genome-wide gene regulatory networks," *IEEE Transactions on Parallel and Distributed Systems*, vol. 21, no. 12, pp. 1721–1733, 2010.

[3] J. Lee Rodgers and W. A. Nicewander, "Thirteen ways to look at the correlation coefficient," *The American Statistician*, vol. 42, no. 1, pp. 59–66, 1988.

[4] W. K. Pratt, "Correlation techniques of image registration," *IEEE Transactions on Aerospace and Electronic Systems*, no. 3, pp. 353–358, 1974.

[5] L. G. Brown, "A survey of image registration techniques," *ACM computing surveys*, vol. 24, no. 4, pp. 325–376, 1992.

[6] I. Guyon and A. Elisseeff, "An introduction to variable and feature selection," *The Journal of Machine Learning Research*, vol. 3, pp. 1157–1182, 2003.

[7] G. Chandrashekar and F. Sahin, "A survey on feature selection methods," *Computers & Electrical Engineering*, vol. 40, no. 1, pp. 16–28, 2014.

[8] Y. Wang, H. Du, M. Xia, L. Ren, M. Xu, T. Xie, G. Gong, N. Xu, H. Yang, and Y. He, "A hybrid cpu-gpu accelerated framework for fast mapping of high-resolution human brain connectome," *PloS One*, vol. 8, no. 5, p. e62789, 2013.

[9] X. Chen, Y. Ba, L. Ma, X. Cai, Y. Yin, K. Wang, J. Guo, Y. Zhang, J. Chen, X. Guo *et al.*, "Characterization of micrornas in serum: a novel class of biomarkers for diagnosis of cancer and other diseases," *Cell Research*, vol. 18, no. 10, pp. 997–1006, 2008.

[10] P. D'haeseleer *et al.*, "How does gene expression clustering work?" *Nature Biotechnology*, vol. 23, no. 12, pp. 1499–1502, 2005.

[11] D.-J. Chang, A. H. Desoky, M. Ouyang, and E. C. Rouchka, "Compute pairwise manhattan distance and pearson correlation coefficient of data points with gpu," in *ACIS International Conference on Software Engineering, Artificial Intelligences, Networking and Parallel/Distributed Computing*. IEEE, 2009, pp. 501–506.

[12] E. Kijsipongse, C. Ngamphiw, S. Tongsima *et al.*, "Efficient large pearson correlation matrix computing using hybrid mpi/cuda," in *International Joint Conference on Computer Science and Software Engineering*. IEEE, 2011, pp. 237–241.

[13] J. Jeffers and J. Reinders, *Intel Xeon Phi coprocessor high-performance programming*. Newnes, 2013.

[14] Y. Liu, B. Schmidt, and D. L. Maskell, "Msa-cuda: multiple sequence alignment on graphics processing units with cuda," in *IEEE International Conference on Application-specific Systems, Architectures and Processors*. IEEE, 2009, pp. 121–128.

[15] T. Kiefer, P. B. Volk, and W. Lehner, "Pairwise element computation with mapreduce," in *Proceedings of the 19th ACM International Symposium on High Performance Distributed Computing*. ACM, 2010, pp. 826–833.

[16] A. Sarje and S. Aluru, "All-pairs computations on many-core graphics processors," *Parallel Computing*, vol. 39, no. 2, pp. 79–93, 2013.

[17] Y. Liu, A. Wirawan, and B. Schmidt, "Cudasw++ 3.0: accelerating smith-waterman protein database search by coupling cpu and gpu simd instructions," *BMC Bioinformatics*, vol. 14, no. 1, p. 117, 2013.

[18] Y. Liu, T.-T. Tran, F. Lauenroth, and B. Schmidt, "Swaphi-ls: Smith-waterman algorithm on xeon phi coprocessors for long dna sequences," in *IEEE International Conference on Cluster Computing*. IEEE, 2014, pp. 257–265.

[19] M. B. Eisen, P. T. Spellman, P. O. Brown, and D. Botstein, "Cluster analysis and display of genome-wide expression patterns," *Proceedings of the National Academy of Sciences*, vol. 95, no. 25, pp. 14 863–14 868, 1998.

[20] F. Zhao, Y. Qu, J. Liu, H. Liu, L. Zhang, Y. Feng, H. Wang, J. Gan, R. Lu, and D. Mu, "Microarray profiling and co-expression network analysis of lncrnas and mrnas in neonatal rats following hypoxic-ischemic brain damage," *Scientific Reports*, vol. 5, 2015.

[21] S. Ballouz, W. Verleyen, and J. Gillis, "Guidance for rna-seq co-expression network construction and analysis: safety in numbers," *Bioinformatics*, vol. 31, no. 13, pp. 2123–2130, 2015.

[22] B. Issac, N. F. Tsinoremas, and E. Capobianco, "Abstract b1-04: Co-expression profiling and transcriptional network evidences from rna-seq data reveal specific molecular subtype features in breast cancer," *Cancer Research*, vol. 75, no. 22 Supplement 2, pp. B1–04, 2015.

[23] B. Wang, A. M. Mezlini, F. Demir, M. Fiume, Z. Tu, M. Brudno, B. Haibe-Kains, and A. Goldenberg, "Similarity network fusion for aggregating data types on a genomic scale," *Nature Methods*, vol. 11, no. 3, pp. 333–337, 2014.

[24] M. A. Hall, "Correlation-based feature selection for machine learning," Ph.D. dissertation, The University of Waikato, 1999.

[25] G. Forman, "An extensive empirical study of feature selection metrics for text classification," *The Journal of Machine Learning Research*, vol. 3, pp. 1289–1305, 2003.

[26] B. Baharudin, L. H. Lee, and K. Khan, "A review of machine learning algorithms for text-documents classification," *Journal of Advances in Information Technology*, vol. 1, no. 1, pp. 4–20, 2010.